COMMUNICATIONS IN COMPUTATIONAL PHYSICS
Vol. **3**, No. 5, pp. 1100-1116

Commun. Comput. Phys.
May 2008

Poisson-Boltzmann Theory of Bionanosystems

A. Sayyed-Ahmad, Y. Miao and P. Ortoleva*

Center for Cell and Virus Theory, Department of Chemistry, Indiana University, Bloomington IN 47405, USA.

Received 19 October 2007; Accepted (in revised version) 19 October 2007

Available online 18 February 2008

Abstract. The structure and function of BNS (bionanosystems) such as macromolecules, viruses and ribosomes are strongly affected by electrostatic interactions. Yet their supra-million atom size makes them difficult to simulate via a straightforward Poisson-Boltzmann (PB) approach. Here we explore a multiscale approach that results in a coarse-grained PB equation that follows rigorously from the all-atom PB equation. The derivation of the coarse-grained equation follows from an ansatz on the dependence of the electrical potential in two distinct ways, i.e. one reflecting atomic-scale variations and the other capturing nanometer-scale features. With this ansatz and a series expansion of the potential in a length-scale ratio, the coarse-grained PB equation is obtained. This multiscale methodology and an efficient computational methodology provide a way to efficiently simulate BNS electrostatics with atomic-scale resolution for the first time, avoiding the need for excessive supercomputer resources. The coarse-grained PB equation contains a tensorial dielectric constant that mediates the channeling of the electric field along macromolecules in an aqueous medium. The multiscale approach and novel salinity connections to the PB equation presented here should enhance the accuracy and wider applicability of PB modeling.

PACS: 41.20.Cv

Key words: Poisson-Boltzmann equation, multiscale analysis, bionanostructures, viruses, ribosomes, macromolecules.

1 Introduction

Electrostatic interactions play a crucial role in determining the structure and dynamics of proteins and more complex structures (e.g., enzymes, ribosomes and viruses). DNA is overall negatively charged due to phosphate groups, and the inner surface of a viral capsid often has a net positive charge, likely to assist in the import of genetic material

*Corresponding author. *Email addresses:* Abdallah.ssa@gmail.com (A. Sayyed-Ahmad), yimiao@indiana.edu (Y. Miao), ortoleva@Indiana.edu (P. Ortoleva)

during viral self-assembly [1]. These bionanosystems (BNS) reside in an aqueous electrolyte, which affects their conformation, stability, and function due to screening and dielectric channeling. Aqueous physiological media contain many mobile ions (e.g., Cl^-, Na^+, K^+, Mg^{++}, and Ca^{++}) which redistribute to screen the Coulomb potential of the fixed charges on the BNS by creating layers of counter-ions. Orientable or polarizable molecules of the host medium also serve to decrease the electrical forces that determine the structure and function of a BNS and its interaction with other features in the system. This accurate calculation of the electrostatic potential could enhance our understanding of BNS [2]. One could, for example, use such calculations to estimate the solvation energy, find pKa values [3], and titration curves for proteins. One could calculate the electrostatic forces between biomolecules for use in molecular dynamics [4]. In carrying out molecular mechanics computations, it is important to account for the channeling of the electric field along a BNS due to the dielectric constant contrast between the aqueous medium and the interior of a protein, an effect not accounted for in $1/r$ Coulomb computations as in the CHARMM force field. Computational challenges are even greater when attempting to model a whole virus or ribosome for therapeutic design or for liposome-cell surface interaction studies associated with the analysis of nanocapsules for the delivery of drugs, genes or siRNA to diseased cells.

The magnitude of the systems of interest can be illustrated by Fig. 1, which shows the capsid of a native cowpea chlorotic mottle virus (CCMV) with atoms colored by charges on them. Fractional charges are assigned according to the CHARMM27 force field. The capsid with 432,240 atoms consists of 180 chemically identical protein subunits that form a 286-Å-diameter icosahedral shell. Each protein subunit is composed of 190 amino acids taking three quasi-equivalent positions on the virus surface. CCMV is one example of the small icosahedral viruses. A typical BNS involves millions of atoms and hence direct PB modeling would require billion grid node computations. Clearly novel methods are needed. The challenge is even more acute when attempting to use PB to compute forces in a molecular dynamics approach. The objective of this study is to investigate methodologies for simulating such supra-million atom systems.

The PB equation has been traditionally used to find the electrostatic potential around a macromolecule. A PB model ignores the volume of ions in the medium. Therefore, PB equation is valid for dilute ionic solutions with several Debye lengths away from the fixed charges on the mesostructure of interest (i.e. *concentration* $\leq 0.15M$) [5]. This model has been applied to calculate properties of molecules in solution [2]. Extensions of the PB model to account for the mobile ions sizes and correlations have been developed [6, 7]. The PB model accounts for solvent molecules implicitly via the dielectric constant ε; ε is low within the molecule, and is assumed to increase gradually to the unperturbed, far field value over several angstroms away from the molecule of interest [8]. Solutions to simple problems with spherical, cylindrical or planar symmetry are available for the linearized PB equation [9, 10]. A closed form formula for the solution of nonlinear PB does not seem to be possible except for the planar case [11] and the infinite cylindrical symmetric case where only counter ions exist in the solution [12].

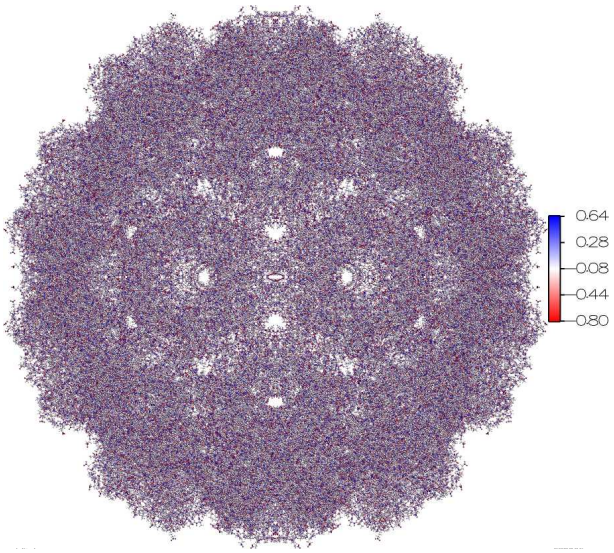

Figure 1: Native CCMV capsid with atoms colored by their charges. Fractional charges are assigned according to the CHARMM27 force field.

In attempting to use numerical methods to solve the PB equation with complicated molecular geometries and charge distributions, a number of challenges present themselves. The equation is highly nonlinear due to the exponential dependence of the mobile ion concentrations on the potential. The electrical potential varies on more than one length scale. The associated characteristic lengths are the size of an atom, the Debye length and the size of the structure of interest. In addition, the length required for the dielectric constant to reach its far field value has a considerable effect on the potential. In summary, one must solve highly nonlinear, multiple scale equations with thousands to millions of spatial variations when addressing bionanosystems.

Several approaches and numerical codes to solve the linear and nonlinear PB equation have been presented throughout the last decade. An overview of numerical techniques commonly applied to the PB type equations is provided in [13]. For the linear PB, a basis set approach is used to express the electrostatic potential as a linear superposition of basis functions [14]. The electrostatic energy functional is then minimized with respect to the expansion coefficients subject to total charge conservation. The boundary element method utilizes analytical solutions obtained in terms of Green's functions and discretization on the domain surface (molecular surface) are used to compute the potential in the whole domain volume [15, 16]. One of the most common approaches used to solve the linear and the nonlinear PB is the finite difference formulation where spatial derivatives are approximated using neighboring points [17–19]. A successive over-relaxation method has been used to get rapid convergence in solving the linear systems obtained from the finite difference discretization [17]. Recently, the finite element method has been successfully used to solve the PB equation for larger systems. An adaptive multilevel approach

based on tetrahedral elements to create a dense mesh to capture the dielectric discontinuity across the molecular surface has been also used. Although irregular grids can be used in a finite element approach, it is inherently less accurate than regular grid methods due to neighboring large and small elements (unless a gradual increase in the element size is imposed) [20]. Furthermore, one might argue that in a physically relevant model, the dielectric discontinuity is not present; rather ε gradually increases to its unperturbed bulk value with distance from the molecule-medium boundary [19]. Also, regular grids lead to simpler and higher order numerical schemes and they allow implementation of multigrid methods [21]. Tomac and Gräslund [22] demonstrated a multigrid finite volume method for solving a modified PB equation for spherical charged particles. The modified PB equation agrees with the results obtained from Monte Carlo simulations on 1:1 and 2:1 ionic solutions. A pseudo-transient continuation and finite element method [23] has been adapted to solve the nonlinear PB equation to utilize the radiation-hydrodynamic parallel code ICF3D. The approach was demonstrated to give accurate solutions for spherically symmetric systems.

This study is motivated by the need to have fine meshes to resolve the structure of, and the potential distribution around a BNS as suggested in Fig. 1. A novel numerical approach to PB simulation is reviewed in Section 2 that reduces the memory requirement by approximately one order of magnitude in comparison to a Galerkin finite element method. The solution of the nonlinear PB equation is obtained from the time evolution of a diffusion-advection equation where there is no need to use Newton-Raphson-like methods. A verification of the solution obtained from our approach is accomplished by comparison with the solution of a charged spherical particle. Results on the CCMV capsid illustrate the viability of our approach for large systems.

A BNS has at least two distinct characteristic lengths: (1) the typical distance between nearest-neighbor atoms and (2) the size of a virus or other nanostructures. This separation of scales has led to the development of multiscale theories which yielded Fokker-Planck or Smoluchowski equations for the stochastic dynamics of nanoscale structures starting from the Liouville equation [62,63]. Most relevant of these theories in the present context is recent work that started from an all-atom description that included the BNS interior as well as that of the host medium [23–25]. The question arises as to the existence of an analogous approach wherein a coarse-grained PB equation could be derived rigorously from one with all-atom detail via multiscale techniques. Such an approach is presented in Section 3 and holds great promise for analyzing electrostatic interactions within and among bionanostructures.

In this paper we present the following. An efficient numerical method for solving the PB equation is outlined in Section 2, along with results on CCMV capsid and a comparison with other approaches. Prospects for a multiscale analysis of PB problems are given in Section 3. A charge broadening method for accelerating the long-range correlation aspect of numerical calculations in presented in Section 4. An extension of the PB equation for concentrated solutions is presented in Section 5. Conclusions are drawn in Section 6.

2 Direct numerical approach to BNS simulation

Solving the elliptic PB equation in 3D is computationally intensive. To capture the molecule-medium interface, and distinguish the structure of a BNS from its surroundings requires a sufficiently fine grid (e.g., with a 0.5 Å spacing). Solution of the nonlinear PB equation using the finite element method on a hexahedral grid via a conjugate gradient iterative solver with compressed coefficient matrix requires approximately 250 N bytes; where N is the number of nodes in the grid. This translates to a limiting resolution of $\sim 160^3$ on a 1 GB RAM computer.

In our approach [26], we formulate a nonlinear advection-diffusion equation which admits the original elliptic nonlinear PB equation as the long time solution. We start with the variational functional formulation for the elliptic PB equation

$$\Xi[\Phi] = \int_\Omega d^3r \left(\frac{1}{2}\varepsilon |\vec{\nabla}\Phi|^2 - 4\pi \int_0^{\Phi(\vec{r})} d\Phi' \rho(\vec{r},\Phi') \right). \tag{2.1}$$

The PB equation is obtained by minimizing (2.1) with respect to the electrostatic potential, Φ, and assuming that Φ or its derivatives vanish on the boundary of the domain Ω. A Langevin steepest descent approach with the dielectric constant spatial distribution, $\varepsilon(\vec{r})$, was used as a friction coefficient to minimize Ξ

$$\varepsilon(\vec{r})\frac{\partial \Phi}{\partial t} = -\frac{\delta \Xi}{\delta \Phi}. \tag{2.2}$$

Calculating the functional derivative of Ξ with respect to Φ and substituting in (2.2) yields

$$\frac{\partial \Phi}{\partial t} = \nabla^2\Phi + \frac{\vec{\nabla}\varepsilon\cdot\vec{\nabla}\Phi}{\varepsilon} + \frac{4\pi F}{\varepsilon}\sum_{i=1}^{N_{ions}} z_i c_i^\infty \exp(-z_i F\Phi/RT) + \frac{4\pi}{\sigma}\sum_{j=1}^{N_{charges}} q_j \delta(\vec{r}-\vec{r}_j), \tag{2.3}$$

where F is Faraday's constant. c_i^∞ and z_i are the bulk concentration and valence of the i-th ionic specie. q_j and $\vec{r}_j$ are the charge and position of the j-th atom, respectively. Since the PB equation has a unique solution, the steady state solution of this advection-diffusion equation corresponds to the solution of the elliptic PB equation. Despite the simplicity and the modest storage requirements of an explicit forward in time, centered in space (FTCS) integration scheme for solving the advection-diffusion equation, using an FTCS scheme is not efficient as the stability of the time integration is constrained by Courant and Peclet numbers [20]. Therefore, one needs a large number of time steps to reach the steady state solution. On the other hand, although a fully implicit scheme allows one to use much larger time steps, it is memory demanding because of the need to store a large sparse matrix. In order to get the advantages of both techniques, we adapted an operator splitting scheme. A commonly used splitting algorithm is the alternating direction method (ADI) which is a variation of the Crank-Nicholson scheme [24]. Details on our discretization scheme are provided in [25].

To demonstrate the applicability of our approach to large BNS, the CCMV capsid is simulated in a $0.15M$ 1:1 electrolyte medium and its potential profile is determined at 625^3 grid nodes with a grid spacing of 0.5Å. Fig. 2 shows 3D electrostatic potential isosurfaces of -1.0kT/e (red) and +1.0kT/e (blue) for the outer shell (a) and inner surface (b) of the capsid. The outer electrostatic potential surface is found to be predominantly negative with patches of positive potential concentrated at the top of the pentamers and hexamers of protein subunits, while the inner surface is mostly positive, which justifies its interactions with the embedded negatively charged RNA. Above results agree with those reported by Konecny et al. [60] except that larger positive potential patches are found on our outer potential surface. Obtaining the PB solution on CCMV capsid to an accuracy of 0.01kT/e required approximately 4 hours on 16 processors of IBM SP power4 computers located at Indiana University. The efficiencies of our PB solver are not withstanding, there are practical limitations. For example, it is too CPU intensive for exhaustive parameter studies, and certainly to generate forces in a molecular dynamics simulation. However, the methodology presented above does provide an approach to computing the coarse-grained PB equation implied by the multiscale analysis as outlined in the next section.

3 Multiscale approach to nanosystem electrostatics

Multiscale analysis is a powerful methodology that has been applied to a broad spectrum of complex classical [27–38, 62–64] and quantum [39–44] many-body systems, and to reaction/transport/mechanical phenomena in porous media [45–52]. The problems to which it has been applied are usually governed by linear equations, although nonlinear reacting-deforming porous media have been considered [51]. We now explore a multiscale approach to the PB problem designed for BNS applications, and which elucidates the origins of dielectric channeling and the interplay of atomic and supra-nanoscale processes in viral, ribosomal and other BNS.

The supra-million atom BNS involves at least two distinct length scales, i.e., (1) the average size of an atom or the nearest-neighbor-atom distance, and (2) the overall (supra-nanometer) size of the BNS and its major component parts. A natural parameter to express the multiscale character of a BNS is the ratio σ of the smaller-to-larger of these two lengths (Figs. 1 and 3). In the following, we reformulate the PB problem in a multiscale fashion, and explore methods to construct solutions in the limit of small σ.

Let $\vec{r}$ be position in the system expressed in units such that as $\vec{r}$ traverses one atom it moves a distance of about one unit. However, as $\vec{r}$ traverses the BNS, it moves a distance of $\mathcal{O}(\sigma^{-1})$. Thus we introduce a scaled position

$$\vec{R}=\sigma\vec{r}.$$

As $\vec{R}$ traverses the BNS, it moves a distance of about one of its units. We then attempt to construct the electrical potential Φ by expressing its distinct and simultaneous dependencies on $\vec{r}$ and $\vec{R}$, and show that the smallness of σ allows one to discover these two dependencies.

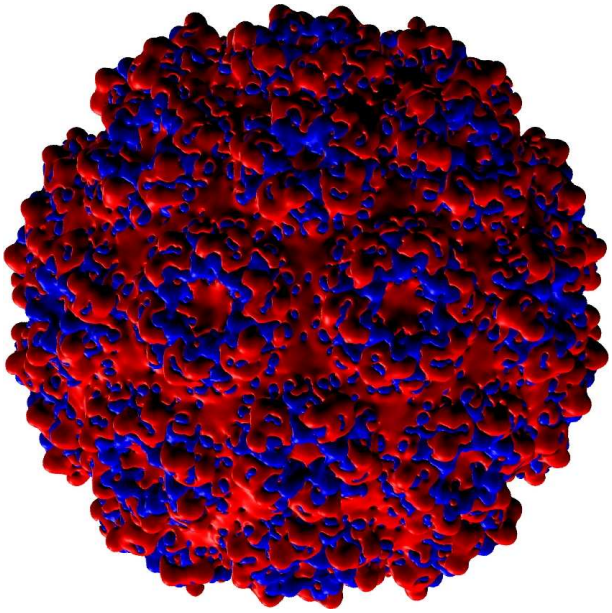

(a)

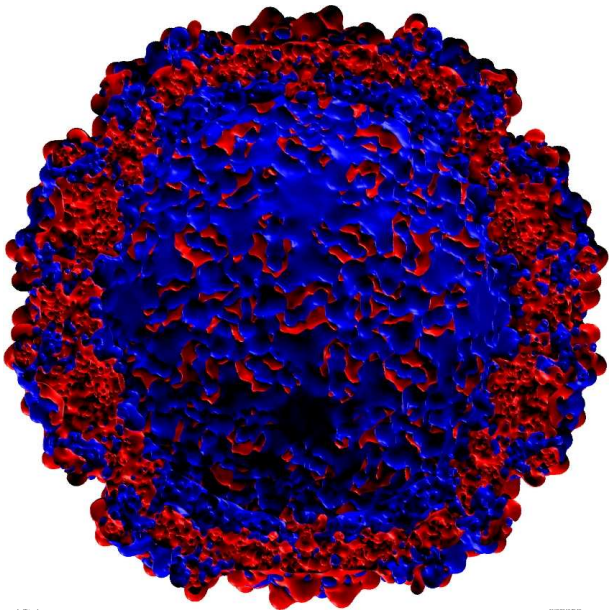

(b)

Figure 2: 3D electrostatic potential isosurfaces of -1.0kT/e (red) and $+$1.0kT/e (blue) for the outer shell (a) and inner surface (b) of the 432,240 atom CCMV capsid immersed in a 0.15M 1:1 electrolyte with a resolution of 625^3, 0.5Å grid spacing.

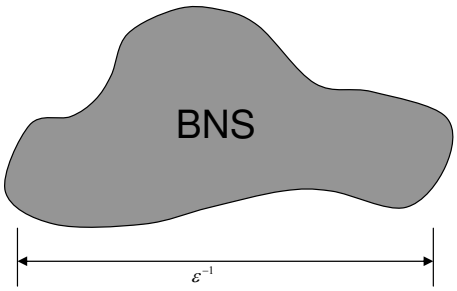

Figure 3: A bionanostructure is $\mathcal{O}(\sigma^{-1})$ in size and contains millions of atoms as suggested in Fig. 1. A multiscale approach that accounts for the widely separated characteristic lengths is developed for solving the PB problem.

Consider the PB model expressed in the $\vec{R}$ spatial scale:

$$\vec{\nabla}\cdot(\varepsilon\vec{\nabla}\Phi)+f=0, \tag{3.1}$$

where ε is the dielectric constant and f is the discrete plus continuous charge density. Both f and ε depend on position, reflecting the underlying fluctuating character of the atomic scale structure, while they also account for the variation in this atomic structure (e.g., the bionanostructure is limited in extent to a zone of size σ^{-1}).

We consider the charge density f to be divided into a continuous part f_c and a discrete part $\sigma^{-1}f_d$. The latter is taken to scale as σ^{-1} to express that near a given fixed charge, its charge density is extremely large, i.e., about one electron charge per cubic angstrom. As the multiscale development unfolds, this σ^{-1} scaling for the discrete charge density is found to yield a self consistent formulation that captures key features of the bionanosystem PB problem.

As Φ depends on both $\vec{r}$ and $\vec{R}$ by our multiscale ansatz, the chain rule implies, upon multiplying (3.1) by σ^2 and letting $\vec{\nabla}_0$ and $\vec{\nabla}_1$ be $\vec{r}$ and $\vec{R}$ gradients respectively,

$$(\vec{\nabla}_0+\sigma\vec{\nabla}_1)\cdot[\varepsilon(\vec{\nabla}_0+\sigma\vec{\nabla}_1)\Phi]+\sigma^2 f_c(\vec{r},\vec{R},\Phi)+\sigma f_d(\vec{r},\vec{R})=0. \tag{3.2}$$

Developing Φ in a power series in σ, and analyzing the equations order-by-order, we construct Φ. To $\mathcal{O}(\sigma^0)$ we obtain

$$\vec{\nabla}_0\cdot(\varepsilon\vec{\nabla}_0\Phi_0)=0.$$

This implies Φ_0 is independent of $\vec{r}$, assuming Φ to be a constant (zero henceforth) at infinity. To $\mathcal{O}(\sigma)$ we obtain

$$\mathcal{L}\Phi_1+\vec{\nabla}_0\cdot(\varepsilon\vec{\nabla}_1\Phi_0)+f_d=0, \tag{3.3}$$

$$\mathcal{L}A=\vec{\nabla}_0\cdot(\varepsilon\vec{\nabla}_0 A), \tag{3.4}$$

for arbitrary r-dependent function A. We find that Φ_1 can be obtained in the form

$$\begin{aligned}&\Phi_1=\vec{b}\cdot\vec{\nabla}_1\Phi_0+\Psi,\\&\vec{\nabla}_0\cdot(\varepsilon\vec{\nabla}_0 b_\alpha)+\partial\varepsilon/\partial r_\alpha=0,\quad \alpha=1,2,3,\\&\mathcal{L}\Psi+f_d=0.\end{aligned}\tag{3.5}$$

Let $b_\alpha=c_\alpha-r_\alpha$, where r_α is the component of $\vec{r}$ along the α direction. Then

$$\vec{\nabla}_0\cdot(\varepsilon\vec{\nabla}_0 c_\alpha)=0.$$

Since b_α must be bounded as $|\vec{r}|\to\infty$ so that Φ_1 is bounded for a BNS in an infinite medium, $c_\alpha\to r_\alpha$ as $|\vec{r}|\to\infty$. This provides the asymptotic condition that uniquely determines c_α, and thus b_α. For the class of problems of interest, $\Phi\to 0$ as $\vec{r}$ and $\vec{R}$ go to infinity, which will be insured via the asymmetric boundary conditions imposed on Φ and the aforementioned conditions on b_α. As b_α is nonzero and fluctuates near and within the zone occupied by the BNS in response to variations in ε, Φ_1 accounts for the atomic-scale aspects of the dielectric channeling of the BNS, while Φ_0 expresses the longer scale channeling. This completes the $\mathcal{O}(\sigma)$ analysis.

To $\mathcal{O}(\sigma^2)$ we obtain

$$\mathcal{L}\Phi_2+\vec{\nabla}_1\cdot(\varepsilon\vec{\nabla}_1\Phi_0)+\vec{\nabla}_0\cdot(\varepsilon\vec{\nabla}_1\Phi_1)+\vec{\nabla}_1\cdot(\varepsilon\vec{\nabla}_0\Phi_1)+f(\vec{r},\vec{R},\Phi_0)=0.\tag{3.6}$$

Integrating over $\vec{r}$, and using the divergence theorem and the conditions at infinity, yields

$$\vec{\nabla}_1\cdot\left[(\vec{\vec{\varepsilon}}^*\vec{\nabla}_1\Phi_0)\right]+f^*(\vec{R},\Phi_0)=0,\tag{3.7}$$

where

$$\begin{aligned}&f^*(\vec{R},\Phi_0)=\langle f\rangle,\quad \langle A\rangle\equiv\Omega^{-1}\int d^3rWA,\\&\varepsilon^*_{\alpha\alpha'}=\langle\varepsilon\rangle\delta_{\alpha\alpha'}+\left\langle\varepsilon\frac{\partial b_{\alpha'}}{\partial r_\alpha}\right\rangle,\end{aligned}$$

for system volume Ω, any $\vec{r}$-dependent quantity A, and W is a weight factor discussed further below. The coarse-grained PB equation yields Φ_0, the long-scale potential profile across the BNS.

The utility of the multiscale PB approach depends on the computational requirements for determining $\vec{b}$ and Φ_0. Since $\vec{b}$ satisfies a linear equation with Dirichlet conditions $\vec{b}=\vec{0}$ at the boundary of the simulations domain, it does not require the costly interaction needed to solve the original nonlinear PB problem. Thus, the development of a multiscale PB solver with greater efficiency than a direct PB approach has great promise. A two grid method is suggested in Fig. 4. The coarse-grained PB equation involves a characteristic length of the BNS size, and not the atomic scale. For a small virus (e.g., CCMV, HRV, poliovirus, HPV) this is roughly 100 times larger in length than the size of an atom. Thus

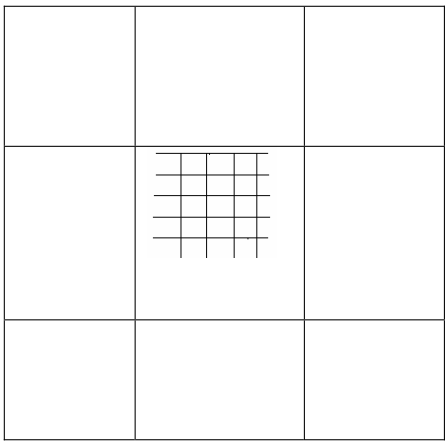

Figure 4: Schematic discretization grid showing the coarse grid, on which the overall potential profile Φ_0 is to be solved, and the fine grid on which the response factor $\vec{b}$ is to be solved.

one can simulate the system with a factor of roughly 10^6 fewer grid points when using the coarse-grained equation for Φ_0, than for the full PB. As CPU time increases supralinearly with the numbers of grid points, this makes multiscale PB up to 10^6 times faster than a direct PB BNS simulation. However, the computation of $\vec{b}$ does introduce some overhead, but this should still be much less costly than a full nonlinear, atomic-scale PB approach.

The modified dielectric factor $\vec{\vec{\varepsilon}}^*$ is a tensor. Its profile across the BNS and the directionality it creates because of its tensorial character account for channeling effects. Also f^* is the coarse-grained charge density. As the system is almost charge neutral within a subvolume of a few cubic nanometers, the range of the weight W in the definition of $\langle\cdots\rangle$ affects f^*. Through W we introduce a finite averaging range of $\mathcal{O}(\sigma^{-1})$ centered on a given value of $\vec{R}$. In that case the developments outlined above proceed when a surface-to-volume argument is used to eliminate $\langle\vec{\nabla}_0\cdot(\varepsilon\vec{\nabla}_0\Phi_2)\rangle$ when arriving at the coarse-grained equations for Φ_0. As Φ_1 captures atomic-scale variations via $\vec{b}$, the multiscale approach retains both short and long scale behaviors — i.e., does not constitute a lumped model wherein atomic-scale variations are lost from the beginning.

4 Ionic strength corrections

The finite volume of ions and the presence of multivalent ions are two main reasons for non-ideal electrolyte behavior at sufficiently high ion concentrations. A good measure that characterizes the range at which ionic solutions deviate from ideal behavior is given by the ionic strength,

$$I=\frac{1}{2}\sum_{i=1}^{N_{ions}} z_i^2 c_i. \tag{4.1}$$

Traditional PB theory has been established to be valid for solutions of very low ionic strengths [4, 53].

Many applications in biomolecular systems involve high concentrations, far from the dilute regime. Therefore, accounting for higher ionic concentrations is crucial considering the fact that the local ion concentrations close to a charged surface or atomic site can exceed 10M in inhomogeneous biomolecular systems. In that regime PB theory does not account for the strongly interacting ions near the surface of a biomolecule. It would be only applicable in the bulk region several Debye lengths away from fixed atomic charges on a BNS. Recall the Debye length is defined by

$$\lambda_{Debye}=\sqrt{\frac{\varepsilon RT}{8\pi F^2 I}}. \tag{4.2}$$

Borukhov and coworkers [54] presented an augmented PB equation that accounts for the finite size of the mobile ions. They used this equation to investigate the adsorption of large ions at highly charged surfaces. However, their modified equation is only derived for 1:z and z:z electrolytes. Tomac and Gräslund [55] demonstrated a multigrid finite volume method for solving a modified PB equation for spherical charged particles. The modified PB equation agrees with the results obtained from Monte Carlo simulations on 1:1 and 2:1 ionic solutions. Here, we introduce a general phenomenological correction to the PB equation that can be used for any electrolyte composition based on utilizing experimentally measured ion activity coefficients in the electrochemical potential:

$$\mu_i=\mu_i^{\theta}(T)+RT\ln\gamma_i c_i+z_i\Phi, \tag{4.3}$$

where γ_i is the activity coefficient of the i-th ion type in the solution. In the asymptotic limit of a dilute electrolyte, the activity coefficient is to unity. In other words, $\gamma_i\to 1$ as all $c_i\to 0$. Furthermore, γ_i depends on the concentration of the ionic specie of type i, as well as the concentration of other ionic species. For instance, in 1M NaCl electrolyte, the activity coefficient of Na^+ is 0.767, while the activity coefficient of Cl^- at the same concentration is 0.599. Similarly, in a 1m NaBr electrolyte, the activity coefficient of Na^+ is 0.684, while that of Cl^- at the same concentration is 0.661 [56]. By applying the activity corrected chemical potential formula, we account for counter-ion crowding near a given charge by redistributing the ions according to the following new calculation algorithm:

$$\gamma_i(c_i)c_i=\gamma_i^{\infty}c_i^{\infty}\exp\left(-\frac{z_iF\Phi}{RT}\right), \tag{4.4}$$

which establishes an implicit nonlinear relationship between c_i and Φ. Denote the solution of the above equation by $c_i^{\mathrm{mod}}(\Phi)$. c_i^{∞} and γ_i^{∞} are the bulk concentration and activity coefficient of i-th ionic specie, respectively. The ionic strength dependence is accounted for through, $\gamma_i(c_i)$, the measured of the activity coefficient of i-th ionic specie as a function of concentration. Despite the long-standing controversy on whether it is possible to determine the activity coefficient of a single ion type, Vera and coworkers have argued

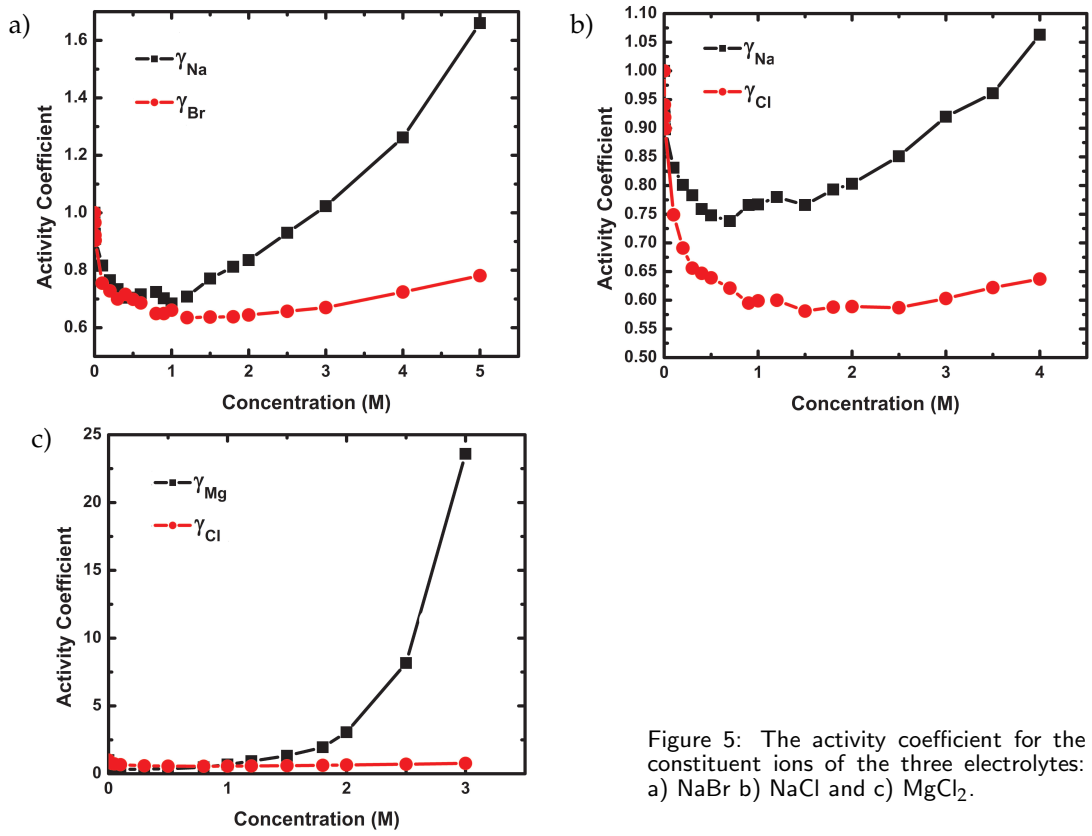

Figure 5: The activity coefficient for the constituent ions of the three electrolytes: a) NaBr b) NaCl and c) $MgCl_2$.

that they developed an experiential technique to do so by using an ion-selective electrode along with a single junction reference electrode, both immersed in the aqueous electrolyte solution of interest. This approach made the measurement of the activity coefficient of single ions possible [56–58]. Fig. 5 shows the activity coefficients for the constituent ions of three ionic solutions [56] for the concentration range $0.1\text{M} - 5.0\text{M}$.

As an illustration, we numerically solve (4.4) for three electrolytes, $MgCl_2$, NaCl and NaBr. We computed $c_i^{\text{mod}}(\Phi)$, the constituent ion concentrations as a function of the electrostatic potential Φ by adopting an extrapolation formula that accounts for activity coefficients at ionic strengths higher than 5.0M:

$$\ln\gamma_i(c_i) = \frac{-A_m z_i^2 I_m^{1/2}}{1+I_m^{1/2}} + \frac{[-B_{m,i} I_m + D_{m,i} I_m^{3/2}]}{1+I_m^{1/2}}, \tag{4.5}$$

where I_m is ionic strength of the electrolyte of type m. A_m is equal to 1.1762. $B_{m,i}$ and $D_{m,i}$ are adjustable parameters obtained by fitting the measured activity coefficients of constituent ions of each solution [61]. Fig. 6 shows a comparison between the concentrations obtained by solving (4.3) and (4.4) with those obtained using the dilute solution theory which is based on a Boltzmann distribution for the mobile ions. When the ab-

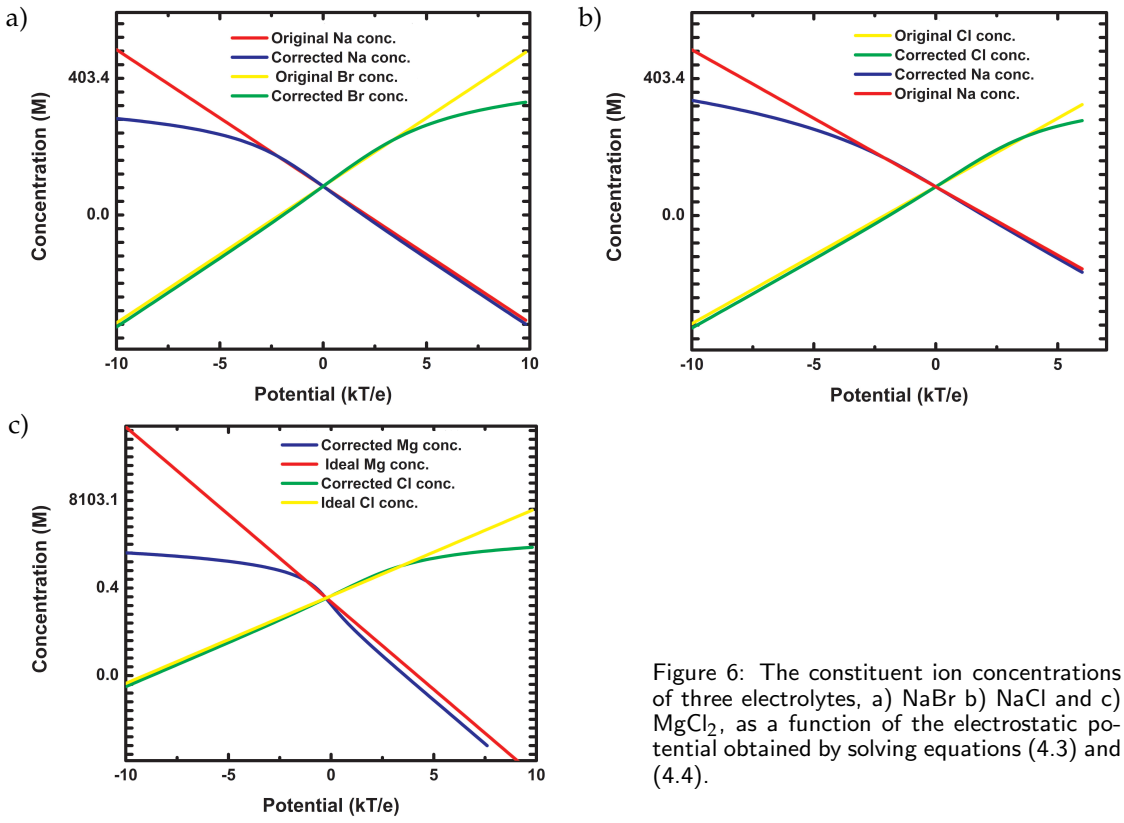

Figure 6: The constituent ion concentrations of three electrolytes, a) NaBr b) NaCl and c) $MgCl_2$, as a function of the electrostatic potential obtained by solving equations (4.3) and (4.4).

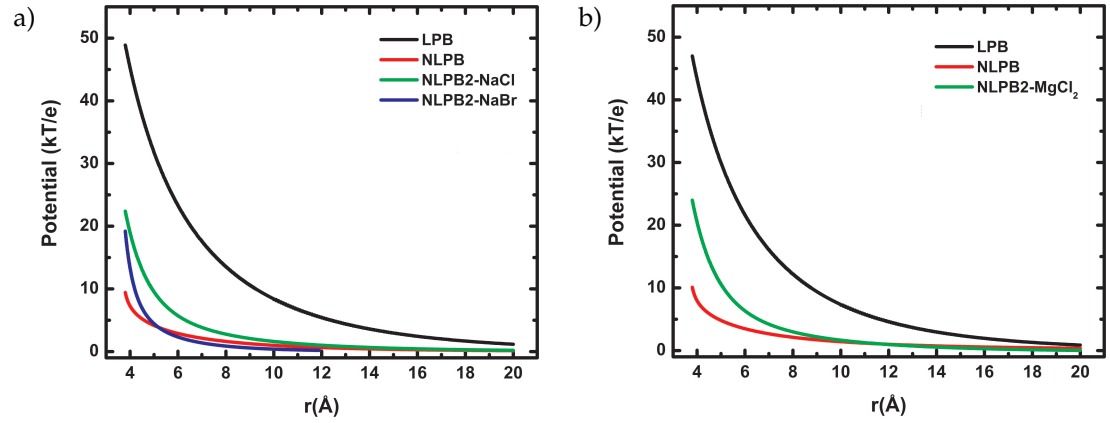

Figure 7: The electrostatic potentials as a function of the radial distance from the center of a 2 Å atom immersed in a) 150mM univalent symmetric electrolyte and b) 75mM electrolyte with divalent ions, as obtained by solving the traditional nonlinear and linear PB as well as the modified nonlinear PB.

solute electrostatic potential is sufficiently large in magnitude (i.e., greater than $4kT/e$ for NaCl and NaBr solutions, and $1kT/e$ for $MgCl_2$ solution), concentrations obtained through the original Boltzmann distribution are considerably higher near an oppositely

charged surface or fixed charge, suggesting that the activity corrected chemical potential was able to account for size, valence and crowding of ions, as well as ion-ion correlations by reducing un-physically high counter-ion concentrations.

Next, we utilize the new relationship between the electrostatic potential and the ionic concentrations shown in Fig. 6 to solve the modified nonlinear PB equation:

$$\nabla\cdot(\varepsilon\nabla\Phi)=-4\pi\left(F\sum_{i=1}^{N_{ions}}z_ic_i^{\rm mod}(\Phi)+q\delta(r)\right). \tag{4.6}$$

We demonstrate the solution of this model for a fixed spherical ion of radius 2 Å and charge +1e in NaBr, NaCl and $MgCl_2$ electrolytes with bulk concentrations of 150mM, 150mM and 75mM, respectively. The dielectric constant inside the fixed charge was assigned a constant value, while the solution dielectric constant was 78.4. An ion-inaccessible layer of 1.8 Å was assigned. Fig. 7 shows the differences among the electrostatic potentials as a function of distance from the center of the fixed ion obtained by solving the modified nonlinear PB equation for NaCl, NaBr and $MgCl_2$ solutions, as well as the original nonlinear and linear PB equations. Clearly, the electrostatic potential obtained using the modified model is quantitatively different from the classic nonlinear and linear PB model results. It tends to decay on a scale longer than that of the potential obtained from the classic nonlinear PB models, and shorter than that obtained from the solution of the classic linear PB model. Furthermore, our modified model produced electrostatic potentials that are quantitatively distinguishable between the results NaCl and NaBr. Such a distinction cannot be attained using the classic PB models.

5 Conclusions

Electrostatic interactions in a BNS can be simulated directly via a nonlinear PB solver. However, the nonlinearity and the need for sub-angstrom-scale numerical grids makes this approach impractical, especially for carrying out parameter studies — i.e., to determine the effect of pH, salinity or temperature on the strength of interactions. Similar comments hold for studies on the effects of mutation or surveying the interactions with a spectrum of putative antiviral or other drugs.

In this study, we presented results on a memory-efficient direct nonlinear PB solver. As a demonstration the capsid of CCMV was used to generate the electrical potential with atomic-scale resolution. To further accelerate PB simulations of a BNS, we introduced a multiscale approach. In the approach we use the multiscale character of BNS to derive rigorous coarse-grained PB models that can be simulated with our nonlinear PB solver. In addition, the multiscale procedure preserves key atomic-scale features of a BNS that takes the form of angstrom-scale spatial variations overlaid on the coarse-grained electrical potential profile. Thus, atomic-scale resolution is preserved, unlike for lumped models wherein subunits (e.g., peptides or nucleotides) are modeled as structureless spheres that cannot compute interactions with a drug molecule without recalibration with each new

application [59]. We also introduced an experimentally inspired, modified PB model that accounts for ion sizes and correlations in a BNS. We demonstrated this approach on a simple spherical particle. The results indicate that our approach can distinguish between different ion types and decrease the unphysical ion crowding near a charged site that arises from the solution of the traditional PB model.

Considering the great promise of multiscale and salinity-corrected PB modeling, we are implementing the approaches of Sections 3 and 4 as a new simulator MS-PB. This package will be available as free open-source software. It will be compatible with standard graphics and molecular manipulation codes, notably VMD [61] and OpenDX, in I/O characteristics.

Acknowledgments

The U.S. Air Force Research laboratories at Wright Patterson Air Force Base provided support through the Oak Ridge Institute of Science and Education (ORISE). The Indiana University College of Arts and Sciences provided support through the Center for Cell and Virus Theory.

References

[1] R. Bruinsma, Eur. Phys. J. E - Soft Matter 19 (2006) 303.
[2] K. Sharp, B. Honig, Ann. Rev. Biophys. Chem. 19 (1990) 301.
[3] C. N. Schultz, A. Warshel, Proteins 44 (2001) 400.
[4] M. K. Gilson, J. A. McCammon, J. D. Madura, J. Comput. Chem. 16 (1995) 1081.
[5] D. A. McQuarrie, Statistical Mechanics, Harper Collins, New York, 1976.
[6] S. Levine, G. M. Bell, J. Phys. Chem. 64 (1960) 1188.
[7] I. Borkukhov, D. Andelman, H. Orland, Phys. Rev. Lett. 79 (1997) 435.
[8] F. Guarnieri, A. B. Schmidt, E. L. Mehler, Int. J. Quant. Chem. 69 (1998) 57.
[9] C. Tanford, Physical Chemistry of Macromolecules, John Wiley and Sons, New York, 1961.
[10] B. I. Shklovskii, Phys. Rev. E 60 (1999) 5802.
[11] P. J. Ortoleva, Mesoscopic Chemical Physics, 2003.
[12] R. M. Fuoss, A. Katchalsky, S. Lifson, Proceedings of the National Academy of Sciences of the United States of America 1951, vol. 37, 579.
[13] R. D. Coalson, T. L. Beck, Numerical methods for solving poisson and Poisson-Boltzmann type equations, in: P. v. R. Schleyer (ed.), Encyclopedia of Computational Chemistry, John-Wiley, New York, 1998, vol. 3, pp 2086.
[14] L. David, M. J. Field, J. Comput. Chem. 18 (1997) 343.
[15] Y. Vorobjev, H. Scheraga, J. Comput. Chem. 18 (1997) 569.
[16] A. J. Bordner, G. A. Huber, J. Comput. Chem. 24 (2003) 353.
[17] A. Nicholls, B. Honig, J. Comput. Chem. 12 (1991) 435.
[18] R. E. Bruccoleri, J. Novotony, M. E. Davis, K. A. Sharp, J. Comput. Chem. 2 (1997) 268.
[19] J. A. Grant, B. Pickup, A. Nicholls, J. Comput. Chem. 22 (2001) 608.
[20] C. A. J. Fletcher, Computational Techniques for Fluid Dynamics, 2nd edition, Springer-Verlag, Berlin, 1988, Vol. I.

[21] M. Holst, F. Saied, J. Comput. Chem. 14 (1993) 105.
[22] S. Tomac, A. Gräslund, J. Comput. Chem. 19 (1998) 893.
[23] A. I. Shestakov, J. L. Milovich, A. Noy, J. Collid Interf. Sci. 247 (2002) 62.
[24] J. J. Douglas, J. E. Gunn, Numer. Math. 6 (1964) 428.
[25] A. Sayyed-Ahmad, K. Tuncay, P. J. Ortoleva, J. Comput. Chem. 25 (2004) 1068.
[26] N. Baker, M. Holst, F. Wang, J. Comput. Chem. 21 (2000) 1319.
[27] S. Chandrasekhar, Astrophys. J. 97 (1943) 255-262.
[28] S. Bose, P. Ortoleva, J. Chem. Phys. 70(6) (1979) 3041-3056.
[29] S. Bose, P. Ortoleva, Phys. Lett. A69(5) (1979) 367-369.
[30] S. Bose, S. Bose, P. Ortoleva, J. Chem. Phys. 72 (1980) 4258-4263.
[31] S. Bose, M. Medina-Noyola, P. Ortoleva, J. Chem. Phys. 75(4) (1981)1762-1771.
[32] J. M. Deutch, I. Oppenheim, Faraday Symp. Chem. S. 83 (1987) 1-20.
[33] P. Ortoleva, Nonlinear Chemical Waves; John Wiley and Sons: New York, 1992.
[34] J. E. Shea, I. Oppenheim, J. Phys. Chem. 100(49) (1996) 19035-19042.
[35] J. E. Shea, I. Oppenheim, Physical A 247(1-4) (1997) 417-443.
[36] M. H. Peters, J. Chem. Phys. 110(1) (1998) 528-538.
[37] M. H. Peters, J. Stat. Phys. 94(3-4) (1999) 557-586.
[38] W. T. Coffey, Y. P. Kalmykov, J. T. Waldron, The Langevin Equation With Applications to Stochastic Problems, in: Physics, Chemistry and Electrical Engineering, World Scientific Publishing Co., River Edge, NJ, 2004.
[39] P. Y. Ayala, G. E. Scuseria, A. Savin, Chem. Phys. Lett. 307(3-4) (1999) 227-234.
[40] J. Almlof, Chem. Phys. Lett. 181(4) (1991) 319-320.
[41] C. J. Cramer, Essentials of Computational Chemistry: Theories and Models, Wiley 2nd edition, 2004.
[42] V. Gognea, L. M. Westerhoff, K. M. Merz Jr., J. Chem. Phys. 113(14) (2000) 5604-5613.
[43] H. Lin, D. Truhlar, Theor Chem Acc, 117(2) (2005) 185.
[44] X. Li, S. A. Hassan, E. L. Mehler, Long Dynamics Simulations of Proteins Using Atomistic Force Fields and a Continuum Representation of Solvent Effects: Calculation of Structural and Dynamic Properties, Wiley-Liss, Inc., 2005, vol 60, no. 3, pp.464-484.
[45] B. Amaziane, A. Bourgeat, J. Koebbe, Numerical simulation of diphasic flow in heterogeneous porous media by homogenization, in: W. E. Fitzgibbon, M. F. wheeler (eds.), Modeling and Analysis of Diffusive and Advective Processes in Geosciences, Philadelphia, SIAM, 1992.
[46] H. Araki, J. Ehlers, K. Hepp, R. Kippenhahn, A. H. Weidenmuller, J. Weiss, J. Zittartz, Homogenization Techniques for Composite Media, Proceedings, Udine, Italy, 1985, Berlin, Springer-Verlag, 1987, p. 397.
[47] A. Bensoussan, J. L. Lyons, G. Papanicolnon, Asymptotic Analysis for Periodic Structures, Amsterdam, North-Holland, 1978.
[48] H. Ene, Application of the homogenization method to transport in porous media, in: J. Cushman (ed.), Dynamics of Fluid in Hierarchical Porous Media, Academic Press, 1990.
[49] U. Hornung, Homogenization of miscible displacement in unsaturated aggregated solids, in: G. D. Maso, G. F. Dell'Antoino (eds.), Composite Media and Homogenization Theory, An International Center for Theoretical Physics Workshop, Irieste, Italy, January 1990, Birkhauser, Boston, 1991.
[50] J. Keller, Effective behavior of heterogeneous media, in: U. Landman (ed.), Statistical Mechanics and Statistical Method in Theory and Application, 1977, pp. 631-644.
[51] C. Qin, P. Ortoleva, Banded diagenetic pressure seals: Types, mechanisms, and homog-

enized basin dynamics, in: P. Ortoleva (ed.), Basin Compartments and Seals, Tulsa, OK AAPG, AAPG Memoir 1994, vol 61, 385-400.
[52] K. Tuncay, P. Ortoleva, Probability functionals, homogenization and comprehensive reservoir simulators, in: J. Chadam, A. Cunningham, R. E. Ewing, P. Ortoleva, M. F. Wheeler (eds.), Resource Recovery, Confinement, and Remediation of Environmental Hazards, Institute of Mathematics and Its Applications, Springer-Verlag, New York, 2002, vol 131, 161-178.
[53] G. Linse, G. Gunnarsson, B. Joensson, J. Phys. Chem. 86 (1982) 413.
[54] I. Borukhov, D. Andelman, H.Orland, Phys. Rev. Lett. 79 (1997) 435.
[55] S. Tomac, A. Gräslund, J. Comput. Chem. 19 (1998) 893.
[56] E. R. J. H. V. Grazyna Wilczek-Vera, AIChE J. 50 (2004) 445.
[57] J. H. V. Mohammad K. Khoshkbarchi, AIChE J. 42 (1996) 249.
[58] G. Wilczek-Vera, E. Rodil, J. H. Vera, Fluid Phase Equilibr. 241 (2006) 59.
[59] D. Zhang, R. Konecny, N. A. Baker, J. A. McCammon, Chem. Soc. 126 (2004) 5897.
[60] R. Konecny, J. Trylska, F. Tama, D. Zhang, N. A. Baker, J. A. McCammon, Biopolymers 82 (2006) 106-120.
[61] W. Humphrey, A. Dalke, K. J. Schulten, Molec. Graphics 14 (1996) 33.
[62] Y. Miao, P. Ortoleva, J. Chem. Phys. 125(4) (2006) 44901.
[63] S. Pankavich, Z. Shreif, P. Ortoleva, Multiscaling for classical nanosystems: Derivation of Smoluchowski & Fokker-Planck equations, submitted.
[64] Y. Miao, P. Ortoleva, J. Chem. Phys. 125(21) (2006) 214901.